Rapid Communications

Isolated frequencies at which nonlinear materials behave linearly

Matthew D. Fronk [*] and Michael J. Leamy [†]
School of Mechanical Engineering, Georgia Institute of Technology, Atlanta, Georgia 30332, USA

(Received 24 September 2019; published 8 November 2019)

In this Rapid Communication, we demonstrate that specific frequencies in weakly nonlinear lattices avoid the generation of higher harmonics, and thus the lattices behave linearly. Using a multiple scales analysis, we present plane-wave solutions that persist at only a single frequency and wave number; i.e., whose spatiotemporal production of higher harmonics is remarkably small. We study monatomic and diatomic chains with quadratic and cubic stiffness nonlinearities as example systems. Direct numerical integration of the equations of motion confirms that finite amplitude plane waves assigned to these special frequencies produce negligible higher harmonics when injected into the lattices. Such findings provide new considerations for the operating frequency of nonlinear communications devices, sensors, and transducers for enhanced signal-to-noise ratios.

DOI: 10.1103/PhysRevE.100.051002

Extensive research has explored the generation of extra-harmonics in nonlinear media, such as those resulting from normal and umklapp phonon scattering processes in anharmonic lattices [1]. Other examples include finite amplitude bulk waves in elastic solids [2–4] and Lamb waves [5–10], which can support second-harmonic synchronization (internally resonant energy exchanges). Similarly, higher-harmonic production has been studied in optical waves for media with nonlinear dielectric coefficients [11], piezoelectric crystals [12], and systems with interfaces [13]. Such problems are posed in a finite, or semifinite, setting by introducing an input boundary condition, commonly harmonic forcing. Recently, wave propagation in periodic media—to include metamaterials—has received increased attention due to their enhanced filtering, cloaking, and waveguiding capabilities. The growth of higher harmonics in forced nonlinear periodic media has also been investigated, with notable recent discoveries of a periodic energy exchange between the forcing frequency and higher harmonics [14], modal mixing between dispersion branches [15], and the formation of subharmonic attenuation zones [16].

By contrast, other studies consider free-wave solutions for infinite nonlinear media. Solution forms include breathers [17–21], solitons [22–28], and cnoidal waves [29–31], which have been observed in water, fiber-optic cables, granular media, and periodic structures. In a recent study, we derived multiharmonic invariant plane-wave solutions for weakly nonlinear lattices using the method of multiple scales [32]. The summation of higher-order solutions composes a multiharmonic plane wave with measurably less growth and decay of its spectral amplitudes, as confirmed by numerical simulations. Such solutions were found to be direction dependent in two-dimensional (2D) shear lattices with symmetric stiffness terms [33]. In this Rapid Communication, we identify special frequencies at which higher-harmonic generation ceases in weakly nonlinear lattices. Such solutions are unique for each lattice design and tunable through wave amplitude, as identified by the multiple scales analysis. Higher amplitudes can be achieved without losing signal information to higher harmonics, thus improving the signal-to-noise ratio at the operating frequency. These findings may inspire new methods for preserving signal integrity in sensors, transducers, and communication devices.

We consider one-dimensional (1D) wave propagation in lattices with physically appropriate, small quadratic and cubic stiffness nonlinearities. This arises in anharmonic three-dimensional crystals when plane waves propagate in the [100], [110], and [111] directions. Analogously, these equations can govern electromagnetic wave propagation in discretized photonic crystals or optical media whereby cubic "stiffness" appears as the Kerr nonlinearity [34–36]. Figures 1(a) and 1(b) present example systems considered herein: nonlinear monatomic and diatomic lattices. The monatomic lattice comprises a single mass m that repeats in each unit cell whereas the diatomic lattice consists of alternating masses m_a and m_b. Both lattices possess linear stiffness denoted by k_1 as well as quadratic and cubic stiffness denoted by k_2 and k_3, respectively. In general, the equations of motion for the jth unit cell of a weakly nonlinear lattice are

$$\mathbf{M}\ddot{\mathbf{x}}_j + \sum_{p=-1}^{+1} [\mathbf{K}^{(p)}\mathbf{x}_{j+p}] + \varepsilon \mathbf{f}_{\mathbf{NL}}(\mathbf{x}_j, \mathbf{x}_{j-1}, \mathbf{x}_{j+1}) = 0, \quad j = -\infty \cdots \infty, \tag{1}$$

where $\mathbf{x}_j$ and $\ddot{\mathbf{x}}_j$ are vectors containing the displacements and accelerations of all masses in the unit cell, respectively; $\mathbf{M}$ and $\mathbf{K}$ denote the mass and stiffness matrices, respectively; and $\mathbf{f}_{\mathbf{NL}}$ consists of the nonlinear restoring forces. The small parameter ε functions as a bookkeeping device in the multiple scales framework. The reader is referred to our prior work for additional details describing higher-order multiple scales analysis of weakly nonlinear 1D [32] and 2D lattices [33].

[*] mfronk3@gatech.edu
[†] michael.leamy@me.gatech.edu

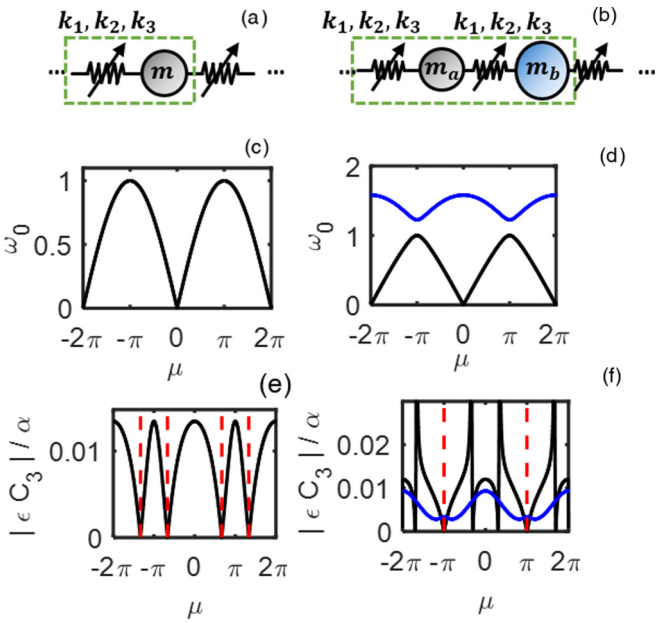

FIG. 1. Schematics of the example lattices considered in this work: nonlinear monatomic (a) and diatomic (b) chains. Weak quadratic and cubic stiffness nonlinearities are studied. Zeroth-order dispersion relationships for the monatomic (c) and diatomic (d) chains. Multiple scales derived third-harmonic solution coefficients for the monatomic (e) and diatomic (f) chains. Specific wave numbers, μ_{null} (identified by vertical dashed lines) exist in which the solution coefficients are identically zero, signifying that higher-harmonic generation is not expected at these special frequencies. For the diatomic chain in (f), only the solution coefficients for the light mass are depicted.

The multiple scales procedure begins by introducing slow timescales and a series solution

$$t = T_0 + \varepsilon T_1 + \ldots \varepsilon^n T_n, \tag{2}$$

$$\mathbf{x}_j = \mathbf{x}_j^{(0)} + \varepsilon \mathbf{x}_j^{(1)} + \cdots + \varepsilon^n \mathbf{x}_j^{(n)}. \tag{3}$$

In accordance with Eq. (2), we define the operator $D_n(\,) \equiv \frac{\partial}{\partial T_n}(\,)$. Collecting terms at matching powers of ε produces a series of cascading differential equations. The first two equations are

$$\varepsilon^0 : \mathbf{M}\ddot{\mathbf{x}}_j^{(0)} + \sum_{p=-1}^{+1} \left[\mathbf{K}^{(p)} \mathbf{x}_{j+p}^{(0)}\right] = 0, \tag{4}$$

$$\varepsilon^1 : \mathbf{M}\ddot{\mathbf{x}}_j^{(1)} + \sum_{p=-1}^{+1} \left[\mathbf{K}^{(p)} \mathbf{x}_{j+p}^{(1)}\right] = -2D_0 D_1 \mathbf{M}\mathbf{x}_j^{(0)} - \mathbf{f}_{\mathbf{NL}}\left(\mathbf{x}_j^{(0)}, \mathbf{x}_{j-1}^{(0)}, \mathbf{x}_{j+1}^{(0)}\right). \tag{5}$$

At the zeroth order, a Bloch wave is admitted, which in its simplest form comprises a single frequency and wave number

$$\mathbf{x}_j^{(0)} = \tfrac{1}{2}\boldsymbol{\phi}(\omega_0) A e^{i\omega_0 T_0} e^{-i\mu j} + \text{c.c.}, \tag{6}$$

where A denotes the wave amplitude, ω_0 the frequency, μ the dimensionless wave number (or propagation constant), $\boldsymbol{\phi}(\omega_0)$ the wave propagation mode shape, and c.c. denotes the complex conjugate of all preceding terms. As depicted in Fig. 1(c), the monatomic lattice possesses a single dispersion branch, whose maximum frequency supporting propagating waves (vis-à-vis evanescent waves) is termed the cut-off frequency. The diatomic lattice in Fig. 1(d), on the other hand, consists of a lower acoustic branch and upper optical branch separated by a band gap.

Updating Eq. (5) with the zeroth-order solution in Eq. (6) gives

$$D_0^2 \mathbf{M}\mathbf{x}_j^{(1)} + \sum_{p=-1}^{+1} \left[\mathbf{K}^{(p)} \mathbf{x}_j^{(1)}\right] = -\mathbf{M} D_1 [i\omega_0 \boldsymbol{\phi}(\omega_0) A e^{i\omega_0 T_0} e^{-i\mu j}] + \sum_{h=0}^{3} \mathbf{a}_{\mathbf{h}}^{(\mathbf{1})} e^{ih(\omega_0 T_0 - \mu j)} + \text{c.c.}, \tag{7}$$

where the $\mathbf{a}_{\mathbf{h}}^{(\mathbf{1})}$ coefficient represents the first-order contribution of each harmonic produced by the nonlinear stiffness interactions. The $\mathbf{a}_{\mathbf{h}}^{(\mathbf{1})}$ coefficients can therefore be expected to depend on the nonlinear stiffness, wave amplitude, and lattice parameters.

Secular terms on the right-hand side of Eq. (7) at $e^{i\omega_0 T_0} e^{-i\mu j}$ (and its complex conjugate) must be eliminated, which yields first-order evolution equations

$$D_1(\alpha) = 0, \tag{8}$$

$$D_1(\beta) = \delta\alpha^2, \tag{9}$$

where α and β are the magnitude and phase, respectively, of the complex amplitude A, and δ is a function of μ, k_3, k_1, and m (if monatomic) or m_a and m_b (if diatomic). As previously studied in [37,38], $D_1(\beta)$ provides closed-form amplitude-dependent corrections to the lattice's zeroth-order band structure. Interestingly, quadratic stiffness does not shift the dispersion curve until higher orders [32,33]. With secular terms eliminated, we seek particular solutions for $\mathbf{x}_j^{(1)}$ that accompany each of the inhomogeneities at $e^{ih(\omega_0 T_0 - \mu j)}$ ($h \neq 1$):

$$\mathbf{x}_j^{(1)} = \sum_{h=0}^{3} \hat{\mathbf{a}}_h^{(1)} e^{ih(\omega_0 T_0 - \mu j)} + \text{c.c.}, \tag{10}$$

where $\hat{\mathbf{a}}_h^{(1)}$ can be obtained through the method of undetermined coefficients. The procedure repeats at each order: removal of secular terms followed by solving for a particular solution. Lattices with quadratic and cubic stiffness possess first-order particular solutions at twice and three times the fundamental frequency and wave number,

$$\mathbf{x}_j^{(1)} = \tfrac{1}{2}\mathbf{B}_2 e^{2i(\omega_0 T_0 - \mu j)} + \tfrac{1}{2}\mathbf{C}_3 e^{3i(\omega_0 T_0 - \mu j)} + \text{c.c.} \tag{11}$$

For the monatomic chain, the coefficients simplify to scalars

$$B_2 = \frac{ik_2 A^2(\sin 2\mu - 2\sin\mu)}{4m\omega_0^2 + 2k_1 \cos 2\mu - 2k_1} = b_2 A^2, \tag{12}$$

$$C_3 = \frac{k_3 A^3(3\cos 2\mu - \cos 3\mu - 3\cos\mu + 1)}{18m\omega_0^2 + 4k_1 \cos 3\mu - 4k_1} = c_3 A^3. \tag{13}$$

The vector expressions for the diatomic chain involve multiple terms, but can be represented symbolically in a similar manner; i.e., $\mathbf{B}_2 = \mathbf{b}_2 A^2$ and $\mathbf{C}_3 = \mathbf{c}_3 A^3$. Note that such waves do not satisfy the zeroth-order dispersion relationship for the lattice; however, they both possess the same *phase velocity* as the zeroth-order solution in Eq. (6). Consequently, the particular solutions summed across all orders compose an invariant plane wave composed of specific magnitudes and phases of higher-harmonic frequencies and wave numbers, valid for all space and time. The inclusion of these very specific higher-order particular solutions results in plane-wave propagation with less spatiotemporal variation of its spectral content. This "shape-preserving" property makes these invariant waves similar to solitons except they are *not* spatially localized solutions.

Figures 1(e) and 1(f) display the magnitude of the third-harmonic solution coefficient $|\mathbf{C}_3|$ as a function of the propagation constant μ for the nonlinear monatomic and diatomic lattices. As expected for these lattice systems, the solution coefficients repeat periodically across the Brillouin zone. For the diatomic lattice, there are propagation constants in which the third-harmonic solution coefficient becomes unbounded. At these frequencies, an internally resonant energy exchange occurs, and the multiple scales analysis requires the inclusion of two plane waves at the zeroth order to capture such energy exchange, which has been the subject of recent work [39]. The aspect we focus on herein is the wave numbers, $\mu = \mu_{\text{null}}$, at which the third-harmonic solution coefficient becomes zero. By extension of the invariance phenomenon, the *absence* of such harmonics leads to a waveform that the nonlinear lattice admits for all space and time, and as such, this higher harmonic can be expected to not develop during propagation. This behavior is quite different from the conventionally studied growth of harmonics in nonlinear waves. Such a finding has implications for the design of sensors, transducers, and communications systems such that they exhibit *linearlike* responses at high-amplitude operation. In applications such as Microelectromechanical System (MEMS) resonators, for example, one might increase input amplitude/power in an attempt to improve the signal-to-noise ratio, but this is often accompanied by nonlinear behavior and loss of information at the sending frequency [40–43]. Operation at $[\mu_{\text{null}}, \omega(\mu_{\text{null}})]$ would avoid this compromise. Additionally, it may be possible to observe ballistic transport of heat-carrying phonons at these special frequencies. From here forward, we restrict our attention to cubic stiffness as quadratic stiffness does not exhibit this phenomenon at propagating wave numbers (those with nonzero group velocity).

As validation of this finding, we carried out direct numerical integration of the lattice equations of motion. Long chains were simulated (e.g., 300 wavelengths for a given value of μ) with viscous dampers whose coefficients increase towards the edge of the structure to absorb reflections. As initial conditions, Eq. (6) (and its corresponding velocity) were assigned to all unit cells at a specific amplitude and frequency and wavenumber combination satisfying the zeroth-order dispersion relationship. The spatial and temporal spectral content of the lattice is then tracked throughout the simulation across time and space. We compare in Fig. 2 the spatiotemporal spectral evolution for two separate simulations of the diatomic

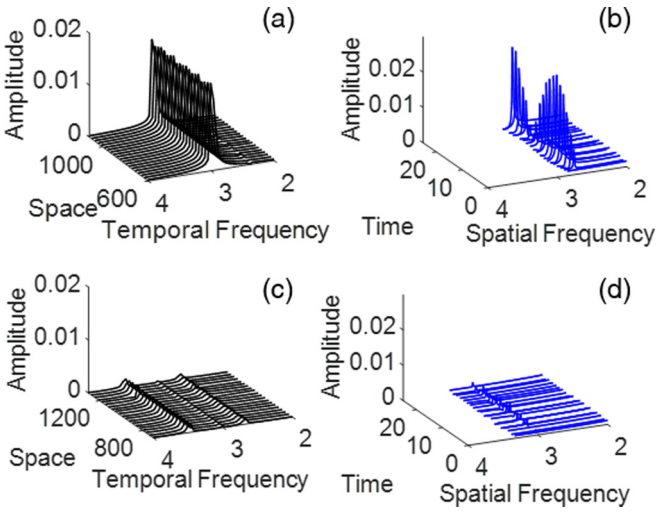

FIG. 2. Spatiotemporal evolution of the spectral content for plane waves in the acoustic branch of the nonlinear diatomic lattice measured in numerical simulations. For lattices given wave numbers away from μ_{null}, higher-harmonic amplitudes develop across space (a) and time (b). By contrast, for lattices assigned plane waves at μ_{null} (predicted by multiple scales), nearly-zero higher-harmonic amplitudes develop across space (c) and time (d). Amplitudes and frequencies are normalized with respect to their values at the fundamental frequency.

lattice: in Figs. 2(a) and 2(b), the lattice is assigned a plane wave away from $[\mu_{\text{null}}, \omega(\mu_{\text{null}})]$; in Figs. 2(c) and 2(d), the lattice is assigned a plane wave at $[\mu_{\text{null}}, \omega(\mu_{\text{null}})]$. In the first case, higher harmonics develop in the temporal and spatial frequency content of the wave, as expected. However, in the latter case, negligible higher-harmonic content develops. Note that the temporal frequency content at approximately $2.67\omega_0$ and $3.46\omega_0$ corresponds to $\omega_0(3\mu)$ for the acoustic and optical branches, respectively.

The procedure is formally repeated over several combinations of initial amplitude and frequency, and the higher-harmonic magnitudes are averaged over many unit cells [for temporal fast Fourier transforms (FFTs)] and time steps (for spatial FFTs). Figure 3 summarizes the results over a range of signal amplitude α. For the monatomic lattice, the measured response of simulated waveforms at $[\mu_{\text{null}}, \omega(\mu_{\text{null}})]$ in Fig. 3(a) is vastly different than those at other frequencies: the magnitudes of higher harmonics are nearly zero regardless of the initial amplitude assigned to the plane wave. This small production of harmonics aligns with the multiple scales prediction of μ_{null} as identified for the monatomic lattice in Fig. 3(b). Since higher-order particular solutions are functions of lower-order particular solutions, still higher-harmonic solution coefficients produced by the cubic stiffness [such as $[5\mu, 5\omega_0(\mu)]$] tend to also evaluate to zero at $[\mu_{\text{null}}, \omega(\mu_{\text{null}})]$.

Additionally, we observe in the nonlinear diatomic lattice in Figs. 3(c)–3(h) that higher-harmonic generation for a single degree of freedom within each unit cell can be blocked. Multiple scales identify frequencies at which $\hat{\mathbf{a}}_3^{(1)} = \begin{bmatrix} \hat{a}_{3,a}^{(1)} \\ 0 \end{bmatrix}$ or $\hat{\mathbf{a}}_3^{(1)} = \begin{bmatrix} 0 \\ \hat{a}_{3,b}^{(1)} \end{bmatrix}$. Thus, there are multiple layers of tunability offered by the diatomic model, as μ_{null} differs based on the degree

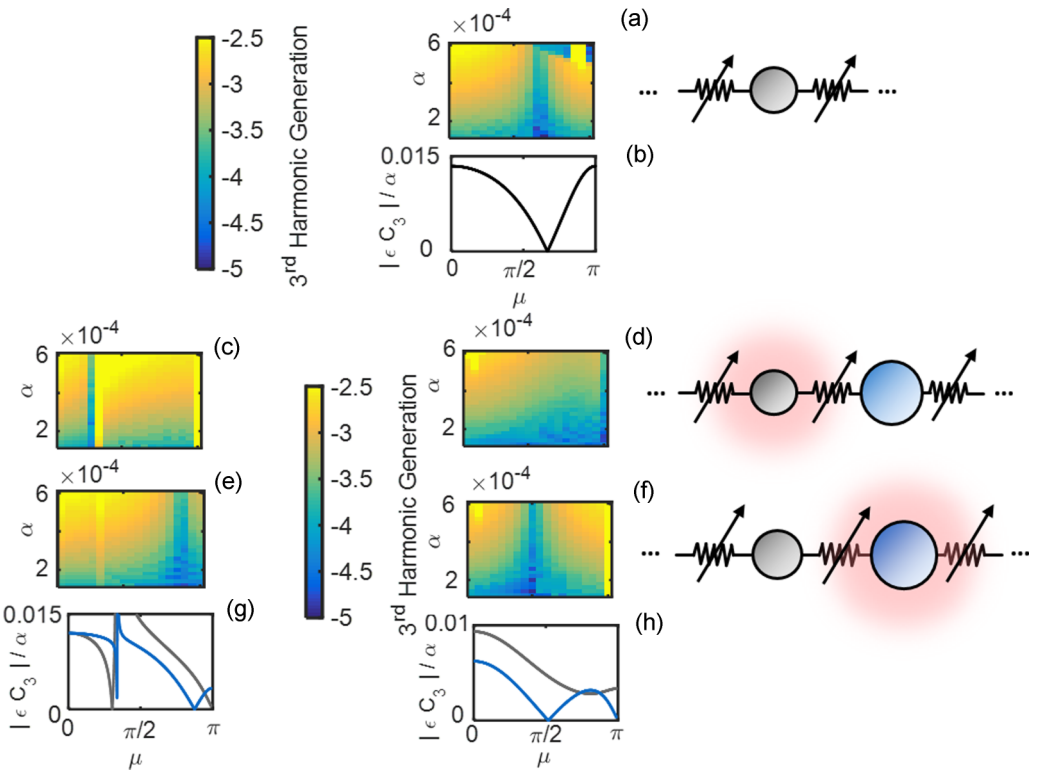

FIG. 3. Third-harmonic generation relative to amplitude α at the fundamental frequency (log-scale) captured by numerical simulations of the nonlinear monatomic lattice (a) compared to the multiple scales predictions of the third-harmonic solution coefficient as a function of the propagation constant (b). Similarly, the third-harmonic production measured in numerical simulations of the diatomic chain is presented for initial conditions at the acoustic branch [(c),(e)] and optical branch [(d),(f)] compared to the perturbation predictions at the acoustic branch (g) and optical branch (h). In (c) and (d) simulations, the light mass is tracked whereas in (e) and (f), the heavy mass is tracked.

of freedom in addition to whether the acoustical or optical branch is excited. This trend is confirmed by the numerical simulations in Figs. 3(c)–3(f), agreeing with perturbation predictions of μ_{null} in Figs. 3(g) and 3(h).

A noteworthy feature of μ_{null} values is that they are independent of the wave's amplitude α. However, due to the amplitude-dependent band structure shifting from the cubic nonlinearity, the temporal frequency $\omega(\mu_{\text{null}})$ grows/shrinks as a function of amplitude, thereby enabling a means to tune the frequency at which the near-zero higher-harmonic generation occurs. Using the closed-form expressions for the amplitude-dependent band structures summarized in Eq. (9), Fig. 4 displays the relationship between $\omega(\mu_{\text{null}})$, the frequency of propagation relative to the first cut-off frequency, and $\Pi_3 \equiv \frac{k_3}{k_1}|A|^2$, the dimensionless strength of the nonlinearity in the system. Because these dispersion corrections apply for weakly nonlinear chains, we restrict Π_3 to $|\Pi_3| \leqslant 0.1$. These plots provide a design strategy for achieving a desired frequency at which higher harmonics should not appear.

Physical insight into the cause of near-zero higher-harmonic generation is difficult to assess. We can extract from Eq. (13) that $\mu_{\text{null}} = \frac{2\pi}{3}$ for the monatomic lattice. Thus, $\omega_0(3\mu_{\text{null}}) = 0$, yielding a zero phase velocity and indeterminate group velocity, which may explain the absence of the third spatial harmonic, 3μ, for the monatomic chain but cannot justify the absence of the third temporal harmonic, $3\omega_0(\mu_{\text{null}})$. For the diatomic chain, $\omega_0(3\mu_{\text{null}}) \neq 0$. More rich behavior may exist for μ_{null} in 2D periodic structures as there may be *directions* in which higher-harmonic generation ceases. Note that the authors recently discovered direction-

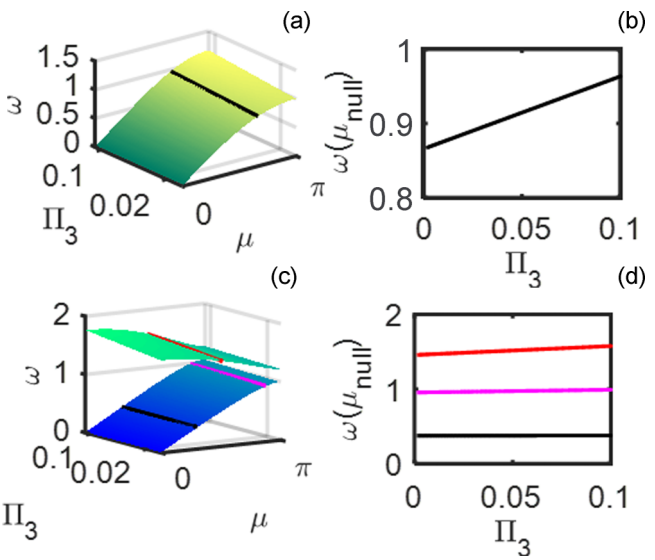

FIG. 4. Analytical, amplitude-dependent dispersion shifting in the monatomic (a) and diatomic (c) lattices. The analytical predictions of dispersion shifting at μ_{null} are evaluated for the monatomic (b) and diatomic (d) lattices to illustrate the tunability of the negligible higher-harmonic generation.

dependent stability and invariance in 2D symmetric shear lattices [33].

In summary, we have found that nonlinear lattices can admit plane waves at specific frequencies which avoid higher harmonics. Such behavior is a dramatic departure from the well-studied phenomenon of higher-harmonic generation of waves in nonlinear media. While the wave number at which this phenomena occurs remains fixed, the frequency varies with wave amplitude as predicted by a multiple scales analysis. Furthermore, lattices with many degrees of freedom per unit cell avoid higher harmonics at different wavelengths, which depend on the degree of freedom considered in each unit cell. This finding may pave the way for inducing linear behavior in nonlinear devices operating at high amplitudes, or achieving near-ballistic thermal transport of phonons at select frequencies.

The authors would like to thank the National Science Foundation for support of this research under Grant No. CMMI 1332862.

[1] C. Kittel, *Introduction to Solid State Physics*, 8th edition (Wiley, New York, 1976), Chap. 4, pp. 89–102.
[2] L. Zarembo and V. Krasil'Nikov, Sov. Phys. Usp. **13**, 778 (1971).
[3] S. Zhou, W. Jiang, and Y. Shui, J. Appl. Phys. **78**, 39 (1995).
[4] Y. Y. Rushchitskii and C. Cattani, Int. Appl. Mech. **38**, 1482 (2002).
[5] M. F. Müller, J.-Y. Kim, J. Qu, and L. J. Jacobs, J. Acoust. Soc. Am. **127**, 2141 (2010).
[6] K. H. Matlack, J.-Y. Kim, L. J. Jacobs, and J. Qu, J. Appl. Phys. **109**, 014905 (2011).
[7] N. Matsuda and S. Biwa, J. Appl. Phys. **109**, 094903 (2011).
[8] Y. Xiang, M. Deng, F.-Z. Xuan, and C.-J. Liu, Ultrasonics **51**, 974 (2011).
[9] Y. Liu, V. K. Chillara, and C. J. Lissenden, J. Sound Vib. **332**, 4517 (2013).
[10] K. Matlack, J.-Y. Kim, L. Jacobs, and J. Qu, J. Nondestr. Eval. **34**, 273 (2015).
[11] E. P. Franken, A. E. Hill, C. Peters, and G. Weinreich, Phys. Rev. Lett. **7**, 118 (1961).
[12] R. C. Miller, Appl. Phys. Lett. **5**, 17 (1964).
[13] Y.-R. Shen, *The Principles of Nonlinear Optics* (Wiley-Interscience, New York, 1984), p. 575.
[14] V. J. Sánchez-Morcillo, I. Pérez-Arjona, V. Romero-García, V. Tournat, and V. E. Gusev, Phys. Rev. E **88**, 043203 (2013).
[15] R. Ganesh and S. Gonella, J. Mech. Phys. Solids **99**, 272 (2017).
[16] P. B. Silva, M. J. Leamy, M. G. D. Geers, and V. G. Kouznetsova, Phys. Rev. E **99**, 063003 (2019).
[17] A. Chabchoub, N. Hoffmann, M. Onorato, and N. Akhmediev, Phys. Rev. X **2**, 011015 (2012).
[18] A. J. Sievers and S. Takeno, Phys. Rev. Lett. **61**, 970 (1988).
[19] S. Takeno and K. Hori, J. Phys. Soc. Jpn. **60**, 947 (1991).
[20] K. W. Sandusky, J. B. Page, and K. E. Schmidt, Phys. Rev. B **46**, 6161 (1992).
[21] D. Chen, S. Aubry, and G. P. Tsironis, Phys. Rev. Lett. **77**, 4776 (1996).
[22] N. J. Zabusky and M. D. Kruskal, Phys. Rev. Lett. **15**, 240 (1965).
[23] A. Hasegawa and F. Tappert, Appl. Phys. Lett. **23**, 142 (1973).
[24] V. Nesterenko, J. Appl. Mech. Tech. Phys. **24**, 733 (1983).
[25] C. Menyuk, IEEE J. Quantum Electron. **23**, 174 (1987).
[26] A. M. Weiner, J. P. Heritage, R. J. Hawkins, R. N. Thurston, E. M. Kirschner, D. E. Leaird, and W. J. Tomlinson, Phys. Rev. Lett. **61**, 2445 (1988).
[27] C. Coste, E. Falcon, and S. Fauve, Phys. Rev. E **56**, 6104 (1997).
[28] C. Daraio, V. F. Nesterenko, E. B. Herbold, and S. Jin, Phys. Rev. E **72**, 016603 (2005).
[29] R. Wiegel, J. Fluid Mech. **7**, 273 (1960).
[30] H. Shin, Phys. Rev. E **63**, 026606 (2001).
[31] G. Friesecke and A. Mikikits-Leitner, J. Dyn. Differ. Eq. **27**, 627 (2015).
[32] M. D. Fronk and M. J. Leamy, J. Vib. Acoust. **139**, 051003 (2017).
[33] M. D. Fronk and M. J. Leamy, J. Sound Vib. **447**, 137 (2019).
[34] F. L. Teixeira, IEEE Trans. Antennas Propag. **56**, 2150 (2008).
[35] C. M. Dissanayake, M. Premaratne, I. D. Rukhlenko, and G. P. Agrawal, Opt. Express **18**, 21427 (2010).
[36] K. Manktelow, M. J. Leamy, and M. Ruzzene, Wave Motion **50**, 494 (2013).
[37] R. K. Narisetti, M. J. Leamy, and M. Ruzzene, J. Vib. Acoust. **132**, 031001 (2010).
[38] K. Manktelow, M. J. Leamy, and M. Ruzzene, Nonlinear Dyn. **63**, 193 (2011).
[39] M. D. Fronk and M. J. Leamy, Phys. Rev. E **100**, 032213 (2019).
[40] V. Kaajakari, T. Mattila, A. Oja, and H. Seppa, J. Microelectromech. Syst. **13**, 715 (2004).
[41] M. Agarwal, S. A. Chandorkar, R. N. Candler, B. Kim, M. A. Hopcroft, R. Melamud, C. M. Jha, T. W. Kenny, and B. Murmann, Appl. Phys. Lett. **89**, 214105 (2006).
[42] A. Tocchio, C. Comi, G. Langfelder, A. Corigliano, and A. Longoni, IEEE Sens. J. **11**, 3202 (2011).
[43] C. Zhao, G. Sobreviela, M. Pandit, S. Du, X. Zou, and A. Seshia, J. Microelectromech. Syst. **26**, 1196 (2017).